Photochemistry and Photobiology, 2005, 81: 983–993

Novel Water-soluble Bacteriochlorophyll Derivatives for Vascular-targeted Photodynamic Therapy: Synthesis, Solubility, Phototoxicity and the Effect of Serum Proteins¶

Alexander Brandis[1], Ohad Mazor[1,2], Eran Neumark[2], Varda Rosenbach-Belkin[1], Yoram Salomon[2] and Avigdor Scherz*[1]

[1]Department of Plant Sciences, The Weizmann Institute of Science, Rehovot, Israel
[2]Department of Biological Regulation, The Weizmann Institute of Science, Rehovot, Israel

Received 1 December 2004; accepted 18 April 2005

ABSTRACT

New negatively charged water-soluble bacteriochlorophyll (Bchl) derivatives were developed in our laboratory for vascular-targeted photodynamic therapy (VTP). Here we focused on the synthesis, characterization and interaction of the new candidates with serum proteins and particularly on the effect of serum albumin on the photocytotoxicity of WST11, a representative compound of the new derivatives. Using several approaches, we found that aminolysis of the isocyclic ring with negatively charged residues markedly increases the hydrophilicity of the Bchl sensitizers, decreases their self-association constant and selectively increases their affinity to serum albumin, compared with other serum proteins. The photocytotoxicity of the new candidates in endothelial cell culture largely depends on the concentration of the serum albumin. Importantly, after incubation with physiological concentrations of serum albumin (500–600 μ*M*), WST11 was found to be poorly photocytotoxic (>80% endothelial cell survival in cell cultures). However, in a recent publication (Mazor, O. *et al.* [2005] *Photochem. Photobiol.* 81, 342–351) we showed that VTP of M2R melanoma xenografts with a similar WST11 concentration resulted in ~100% tumor flattening and >70% cure rate. We therefore propose that the two studies collectively suggest that the antitumor activity of WST11 and probably of other similar candidates does not depend on direct photointoxication of individual endothelial cells but on the vascular tissue response to the VTP insult.

INTRODUCTION

The role of vascular shutdown in the induction of tumor necrosis is now well established and it has provided the motivation for several new avenues of cancer treatment (1–3). Novel methods of antivascular therapy are rapidly being developed for the treatment of solid tumors and nonmalignant diseases associated with abnormal vascularization. The methodology of antivascular therapy is based either on destroying existing blood vessels, preventing the formation of *de novo* neovascularization or inhibiting blood flow (4). All these interventions result in oxygen and nutrient deprivation in the treated tissues, which is expected to cause complete starvation and total necrosis of the malignant cells. Similar treatment modalities are currently aimed at age-related macular degeneration (AMD) (5) and look promising for the treatment of obesity (6).

The antivascular effect of photodynamic therapy (PDT) with some reagents has been recognized for quite some time and has been utilized in several clinical protocols (7). PDT is a relatively new treatment modality whereby nontoxic drugs (sensitizers) and nonhazardous light (VIS/NIR) combine to generate cytotoxic reactive oxygen species (ROS) at a selected treatment site. Numerous experiments have indicated that tumor regression and cure after most PDT treatment protocols involve the occlusion and/or perforation of blood vessels (8–12), in addition to the direct killing of tumor cells. This effect is more pronounced in treatment protocols that involve short light/drug intervals and/or more hydrophilic sensitizers (13). Differences between the response of the tumor and the normal tissue vasculature may provide the key in selecting the best treatment (14–22).

In looking for a more effective and selective vascular-targeted PDT (VTP), we have synthesized new bacteriochlorophyll (Bchl) derivatives (23). These new derivatives present minimal extravasation from the circulation (24,25) and therefore should confine ROS generation to the vascular compartment of the illuminated tissue. Chen *et al.* (26) recently reviewed several of these compounds. Their illumination at the highest concentration in the blood (shortly after bolus administration or after approaching a steady-state concentration following perfusion [27]) resulted in a very rapid occlusion of tumor blood vessels and a markedly slower occlusion of normal blood vessels (19,28). Pd-bacteriopheophorbide (Pd-Bpheid, Tookad®) is the first of these drugs to enter clinical trials (Phase II) for treating local recurrent prostate cancer after failed radiation. However, vascular destruction with Tookad®, as with several other PDT reagents, was shown to involve hemorrhagic necrosis (29), which may induce nondesirable effects when applied to certain tumor sites such as the brain and lungs. Moreover, hemorrhagic necrosis may induce local inflammation and the subsequent proliferation of neovessels, which may retard the

¶Posted on the website on 19 April 2005
*To whom correspondence should be addressed: Prof. Avigdor Scherz, Dept. of Plant Sciences, Weizmann Institute of Science, Rehovot 76100 Israel. Fax: 972-8-9344181; e-mail: avigdor.scherz@weizmann.ac.il
Abbreviations: Bchl, bacteriochlorophyll; FCS, fetal calf serum; Pd-Bpheid, palladium-bacteriopheophorbide; PDT, photodynamic therapy; ROS, reactive oxygen species.

therapeutic effect (4). Thus, VTP, which causes vascular shutdown while minimizing the direct destruction of endothelial cells and the subsequent infarction of the blood vessels, is desirable under some circumstances.

To explore this possibility and its practical implications, we decided to synthesize a number of hydrophilic Bchl derivatives that cause minimal photodamage to endothelial cells under physiologically relevant conditions *in vitro* but still maintain high VTP efficacy *in vivo*. The synthesis of hydrophilic Bchl derivatives was performed via aminolysis of the Bchl isocyclic ring. This reaction was shown to be simple and regioselective when used for the synthesis of chlorophyll (Chl) amide derivatives at the C-13[1] position (30–37). The obtained compounds appeared to be highly water-soluble as well as potent antivascular sensitizers. Here we describe the synthesis, solubility and affinity of serum proteins and the spectral properties of the new compounds in aqueous solutions as well as their photocytotoxicity against endothelial cell lines with different concentrations of serum proteins. In a previous manuscript (38), we reported on the biological activity of WST11, a representative of this new group of photosensitizers, selected for clinical trials (24,38). The previous report describes the cellular trafficking, biodistribution, pharmacokinetics and PDT of M2R melanoma xenografts. Remarkably, Mazor *et al.* (38) showed that the representative water-soluble Bchl-based sensitizer (WST11), which was found to be practically nonphototoxic against individual cells in cultures in physiological serum albumin concentrations, is highly active as a VTP reagent. In a view of these observations, we think that WST11 and other similar compounds of that family, which are relatively nonphototoxic to the endothelial cells but possess potent antitumor activity, are good candidates for VTP, particularly when hemorrhagic necrosis is undesirable.

MATERIALS AND METHODS

Materials. 3-Amino-1-propane sulfonic acid (homotaurine, Aldrich, Milwaukee, WI), 2-aminoethane sulfonic acid (Taurine, Sigma, St. Louis, MO), *N*-hydroxysulfosuccinimide (sulfo-NHS, Pierce, Rockford, IL), 1-(3-dimethylaminopropyl)-3-ethylcarbodiimide (EDC, Fluka, Buchs SG, Switzerland).

Methods. Thin-layer chromatography (TLC) was performed on silica plates (Kieselgel-60, Merck, Darmstadt, Germany). System A: chloroform-methanol (80:20, v/v); system B: chloroform-methanol-water (65:30:0.4, v/v).

Column adsorption chromatography was performed with silica (70/200 mesh, Kieselgel-60, Merck).

^{1}H Nuclear magnetic resonance (NMR) spectra were recorded on Avance DPX 250 and 400 instruments (Bruker, Rheinstetten, Germany) and reported in parts per million (δ) downfield from tetramethylsilane with residual solvent peaks as the internal standards.

Optical absorption spectra were routinely recorded with Genesis-2 (Milton Roy, Berkshire, England). More accurate measurements, *e.g.* for performing factor analysis as described below, were performed with a Cary-5E instrument (Varian, Palo Alto, CA) by using 0.1, 2 and 10 mm path length quartz cells.

Circular dichroism spectra were recorded by an Aviv-202 CD spectrometer (Aviv Instruments, Inc., Lakewood, NJ) by using rectangular quartz cells with a 5 and 10 mm path length.

For determining the extinction coefficients of the Pd-, Cu-, Zn- and Mn-containing derivatives, the metal concentration determined by the previously described ICP-AES methodology (SpectroFlame, Spectro, Kleve, Germany) was correlated with the optical density of the examined solution at the particular wavelength (39), assuming one metal ion per macrocycle.

The hydrophobicity values of the compounds were expressed in terms of their partition coefficient (P) between *n*-octanol:water and determined as recently described (40).

Electrospray ionization mass spectra (ESI-MS) were recorded on a platform LCZ spectrometer (Micromass, Manchester, England).

High-performance liquid chromatography (HPLC) was carried out using a LC-900 instrument (JASCO, Tokyo, Japan) equipped with a MD-915 diode-array detector. Column: ODS-A 250 × 20 S10P-μm column (YMC, Kyoto, Japan).

The partition of photosensitizers among serum proteins was estimated by the following steps.

(1) Preparation of photosensitizer-serum protein complexes. Two hundred microliters of Tookad® (a micellar solution of **3** in aqueous medium at 2.5 mg/mL stabilized with Cremophor EL®, provided by Negma-Lerads, Magny-Les-Hameaux, France; batch no. 56D05002, lot no. 02120) and 180 μL of aqueous solution of **10** (4 m*M*) were incubated with fetal calf serum (FCS, 0.6 mL; Kibbutz Beit Haemek, Israel) at 37°C in the dark for 10 min. The mixtures were loaded onto PD-10 columns containing Sephadex G-25 M (Pharmacia, Biotech, Piscataway, NJ) and eluted by using phosphate-buffered saline (PBS) (pH 7.4, containing 4.7 m*M* ethylenediaminetetraacetic acid [EDTA]) or TBE (89 m*M* Tris-borate, pH 8.3, 2 m*M* EDTA) buffer, both stabilized with 0.2% sodium azide. The fast-running colored zone containing sensitizer-protein complexes was collected for further analysis. The sensitizer's recovery was estimated spectrophotometrically (Genesis-2, Milton Roy) in 93% methanol/TBE buffer (for **3**) and 50% methanol/TBE buffer (for **10**).

(2) Size-exclusion chromatography. Size-exclusion chromatography was performed by using a Superose 6 HR 10/30 (Pharmacia, Biotech) column, connected to a HPLC system. Elution was performed with PBS or a TBE buffer at a flow rate of 0.4 mL/min (41,42). After primary equilibration of the column (two column volumes with the buffer), the sample (250 μL) was injected. Fetal high-density lipoprotein (HDL), obtained from serum ultracentrifugation (43) and bovine serum albumin (BSA) (Sigma, catalogue no. A 2153) was used for calibration (see Fig. 6a). The elution profile was monitored by using a diode-array detector at a 220–900 nm spectral range.

Determining the sensitizer-BSA association was carried out by the interaction of BSA with increasing amounts of **10**. Concentrations in PBS (0.5 mL) after mixing: BSA, 10 μ*M*; compound **10**, 2, 5, 10, 20 and 50 μ*M*. The mixtures were briefly vortexed, incubated for 5 min at 37°C and 0.5 h at room temperature, loaded onto PD-10 (Sephadex G-25) columns and prewashed with 25-mL portions of TBE buffer. The associates were eluted with 6-mL portions of TBE buffer. The obtained eluates were frozen and lyophilized overnight. The dry residues were extracted with methanol (2 mL for each sample). The extracts were centrifuged in 2-mL microtubes to remove insoluble material and the amounts of sensitizer were determined spectophotometrically.

Factor analyses were performed following Noy *et al.* (44). Samples containing different concentrations of tested sensitizers (1 μ*M*–3 m*M*) or BSA (0–1 m*M*) were prepared.

Synthesis. Bacteriochlorophyll a (Bchl a) (1) was extracted and purified from lyophilized cells of *Rhodovolum sulfidophilum* as previously described (23).

Bacteriopheophorbide a (Bpheid, **2**) and *palladium bacteriopheophorbide a* (Pd-Bpheid, **3**, Tookad®) were prepared as described (45 and 23, respectively).

Palladium bacteriochlorin 13^1-(3-sulfopropyl)amide dipotassium salt (5). Homotaurine (30 mg) dissolved in 1 mL of 1 *M* K_2HPO_4 (pH adjusted with HCl to 8.2) was added to a solution of Pd-Bpheid (**3**) (20 mg) in dimethyl sulfoxide (DMSO) (3 mL) while stirring and argon was bubbled into the solution. Then, the reaction mixture was completely dried after a 40 min evaporation at 1–2 millibar and 35°C (Rotavapor R-134, Büche, Switzerland). The solids were redissolved in 7 mL of MeOH, and the colored solution was filtered through cotton wool to remove buffer salts and excess taurine. Next, the methanol was evaporated and the product **5**, redissolved in water, was purified by HPLC, applying 5% methanol in 5 m*M* phosphate buffer at pH 8.0 as solvent A and methanol as solvent B using gradient elution: B, 45% (0 min), 70% (14 min), 100% (16–18 min), 45% (24 min), with a flow rate of 12 mL/min from 0 to 14 min and thereafter at 6 mL/min. The product **5** was eluted and collected in ~9–11 min. The main impurities, collected after 4–7 min (*ca* 3–5%), corresponded to Schiff base by-product(s). The peaks at 22–25 min (*ca* 1–2%) possibly corresponded to the isoform of the main product **5** and the untreated Pd-Bpheid residues. The purified product **5** was dried under reduced pressure, then redissolved in methanol (3 mL) and filtered from insoluble material. Finally, the solvent was evaporated again and the solid compound **5** was stored under argon atmosphere in the dark at –20°C. Yield: 23 mg (87%). ESI-MS (–): 889 (M^--K-H), 873 (M^--2K-H+Na), 851 (M^--2K), 819 (M^--2K-H-OMe) *m/z*. ^{1}H NMR in methanol-d_4, δ: 9.36 (5-H, s), 8.74 (10-H, s),

8.54 (20-H, s), 5.30 and 4.93 (15^1-CH_2, dd), 4.2–4.4 (7,8,17,18-H, m), 3.85 (15^3-Me, s), 3.50 (2^1-Me, s), 3.16 (12^1-Me, s), 3.05 (3^2-Me, s), 1.90–2.40, 1.56–1.74 (17^1, 17^2-CH_2, m), 2.14 (8^1-CH_2, m), 1.90 (7^1-Me, d), 1.59 (18^1-Me, d), 1.08 (8^2-Me, t), 3.57, 3.03 and 2.77 (CH_2s of homotaurine). UV-VIS in methanol ($\varepsilon \times 10^5\ M^{-1}cm^{-1}$): 747 (1.21), 516 (0.16), 384 (0.50), 330 (0.61) nm.

Palladium bacteriopheophorbide a 17^3-(3-sulfo-1-oxy-succinimide)ester sodium salt (6). Fifty milligrams of Pd-Bpheid (**3**), 80 mg of *N*-hydroxysulfosuccinimide (sulfo-NHS) and 65 mg of 1-(3-dimethylaminopropyl)-3-ethylcarbodiimide (EDC) were mixed in 7 mL of dry DMSO overnight at room temperature under argon atmosphere. Next, the solvent was evaporated under reduced pressure. The dry residue was redissolved in chloroform (50 mL), filtered from the insoluble material and evaporated. The conversion was ~95% (TLC). The product **6** did not undergo further chromatographic purification. ESI-MS (–): 890 (M^--Na) *m/z*. ^{1}NMR in chloroform-*d*, δ: 9.19 (5-H, s), 8.49 (10-H, s), 8.46 (20-H, s), 5.82 (13^2-H, s), 4.04–4.38 (7,8,17,18-H, m), 3.85 (13^4-Me, s), 3.47 (2^1-Me, s), 3.37 (12^1-Me, s), 3.09 (3^2-Me, s), 1.77 (7^1-Me, d), 1.70 (18^1-Me, d), 1.10 (8^2-Me, t), 4.05 (CH_2 of sNHS), 3.45 (CH of sNHS).

Palladium bacteriopheophorbide a 17^3-(3-sulfopropyl) amide potassium salt (7). Activated ester **6** (10 mg) in DMSO (1 mL) was mixed with homotaurine (20 mg) in 0.1 *M* K-phosphate buffer, pH 8.0 (1 mL) overnight. Next, the reaction mixture was evaporated. Finally the residue was redissolved in chloroform-methanol (19:1) and the product **7** was purified by chromatography on silica using chloroform-methanol (4:1, v/v) as an eluent. Yield: 8 mg (83%). ESI-MS (–): 834 (M-K) *m/z*. ^{1}NMR in chloroform-*d*/methanol-d_4 (4:1, vol.), δ: 9.16 (5-H, s), 8.71 (10-H, s), 8.60 (20-H, s), 6.05 (13^2-H, s), 4.51, 4.39, 4.11, 3.98 (7,8,17,18-H, all m), 3.92 (13^4-Me, s), 3.48 (2^1-Me, s), 3.36 (12^1-Me, s), 3.09 (3^2-Me, s), 2.02-2.42 (17^1 and 17^2-CH_2, m), 2.15 (8^1-CH_2, q), 1.81 (7^1-Me, d), 1.72 (18^1-Me, d), 1.05 (8^2-Me, t), 3.04, 2.68 and 2.32 (CH_2 of homotaurine, m).

Palladium bacteriochlorin 13^1,17^3-di(3-sulfopropyl)amide dipotassium salt (8). Ten milligrams of compound **6** or **7** were dissolved in 3 mL of DMSO, mixed with 100 mg of homotaurine in 1 mL of 0.5 *M* K-phosphate buffer, pH 8.2, and incubated overnight at room temperature. The solvent was then evacuated under reduced pressure and the product **8** was purified on HPLC as described above for **5**. Yield: 9 mg (81%). ESI-MS (–):1011 (M^--K), 994 (M^--2K+Na), 972 (M^--2K), 775 (M^--2K-CO_2Me-homotaurine $NHCH_2CH_2CH_2SO_3$), 486 ([M-2K]/2) *m/z*. ^{1}NMR in methanol-d_4, δ: 9.35 (5-H, s), 8.75 (10-H, s), 8.60 (20-H, s), 5.28 and 4.98 (15^1-CH_2, dd), 4.38, 4.32, 4.22, 4.15 (7,8,17,18-H, all m), 3.85 (15^3-Me, s), 3.51 (2^1-Me, s), 3.18 (12^1-Me, s), 3.10 (3^2-Me, s 2.12-2.41 (17^1-CH_2, m), 2.15–2.34 (8^1-CH_2, m), 1.76–2.02 (17^2-CH_2, m), 1.89 (7^1-Me, d), 1.61 (18^1-Me, d), 1.07 (8^2-Me, t), 3.82, 3.70, 3.20, 3.10, 2.78, 2.32, 1.90 (CH_2 of homotaurine at C-13^1 and C-17^3). UV-VIS in methanol ($\varepsilon \times 10^5\ M^{-1}\ cm^{-1}$): 747 (1.26), 516 (0.17), 384 (0.51), 330 (0.63) nm.

Palladium 3^1-(3-sulfopropylimino)bacteriochlorin 13^1,17^3-di(3-sulfopropyl)amide tripotassium salt (9). Compound **9** was separated as a minor by-product (*ca.* 3%) during synthesis of **8** and separated by HPLC. HPLC was used in a second cycle of purification of **5**, but with 10–15% gradient of B in a 0–14 min interval. ESI-MS (–): 1171 (M^--K+H), 1153 (M^--2K-H+Na), 1131 (M^--2K), 566 ([M^--K]/2), 364 ([M^--3K]/3) *m/z*. ^{1}NMR in methanol-d_4, δ: 8.71 (1H), 8.63 (1.5H), 8.23 (0.5H) (5-, 10- and 20-H, all-m), 5.30 and 4.88 (15^1-CH_2, dd), 4.43 and 4.25 (7,8,17,18-H, m), 3.85 (15^3-Me, s), 3.31 (2^1-Me, s), 3.22 (12^1-Me, s), 3.17 (3^2-Me, m), 1.89–2.44 (17^1 and 17^2-CH_2, m), 2.25 (8^1-CH_2, m), 1.91 (7^1-Me, s), 1.64 (18^1-Me, s), 1.08 (8^2-Me, t), 4.12, 3.56, 3.22, 3.16, 2.80 and 2.68 (CH_2 of homotaurine). UV-VIS in methanol ($\varepsilon \times 10^4\ M^{-1}\ cm^{-1}$): 729 (9.00), 502 (0.90), 380 (5.44), 328 (5.13).

Palladium bacteriochlorin 13^1-(2-sulfoethyl)amide dipotassium salt (10, WST11). Taurine (1.3 g) dissolved in 40 mL of 1 *M* K_2HPO_4 (pH adjusted to 8.2 with HCl) was added to Pd-Bpheid **3** (935 mg) in DMSO (120 mL) while stirring under bubbled argon. Purification was carried out as described for **5**. Yield: 1.07 g (89%). ESI-MS (–): 875 (M^--K-H), 859 (M^--2K-H+Na), 837 (M^--2K), 805 (M^--2K-H-OMe), 719 *m/z*. ^{1}H NMR in methanol-d_4, δ: 9.38 (5-H, s), 8.78 (10-H, s), 8.59 (20-H, s), 5.31 and 4.95 (15^1-CH_2, dd), 4.2-4.4 (7,8,17,18-H, m), 3.88 (15^3-Me, s), 3.52 (2^1-Me, s), 3.19 (12^1-Me, s), 3.09 (3^2-Me, s), 1.92-2.41, 1.60-1.75 (17^1, 17^2-CH_2, m), 2.19 (8^1-CH_2, m), 1.93 (7^1-Me, d), 1.61 (18^1-Me, d), 1.09 (8^2-Me, t), 3.62, 3.05 (CH_2 of taurine). UV-VIS in methanol ($\varepsilon \times 10^5\ M^{-1}\ cm^{-1}$): 747 (1.20), 516 (0.16), 384 (0.49), 330 (0.60) nm.

Bacteriochlorin 13^1-(2-sulfoethyl)amide dipotassium salt (11). Taurine (160 mg) dissolved in 5 mL of 1 *M* K_2HPO_4 (pH adjusted to 8.2 as above) was added to Bpheid **2** (120 mg) dissolved in 15 mL of DMSO. The reaction and purification continued as described for **5**. Yield: 138 mg (87%). ESI-MS (–): 734 (M^--2K) *m/z*. NMR in methanol-d_4, δ: 9.31 (5-H, s), 8.88 (10-H, s), 8.69 (20-H, s), 5.45 and 5.25 (15^1-CH_2, dd), 4.35 (7,18-H, m), 4.06 (8,17-H, m), 4.20 and 3.61 (2-CH_2, m of taurine), 3.83 (15^3-Me, s), 3.63 (2^1-Me, s), 3.52 (3-CH_2, m of taurine), 3.33 (12^1-Me, s), 3.23 (3^2-Me, s), 2.47 and 2.16 (17^1-CH_2, m), 2.32 and 2.16 (8^1-CH_2, m), 2.12 and 1.65 (17^2-CH_2, m), 1.91 (7^1-Me, d), 1.66 (18^1-Me, d), 1.07 (8^2-Me, t). UV-VIS in methanol ($\varepsilon \times 10^4\ M^{-1}\ cm^{-1}$): 747 (6.30), 519 (1.89), 354 (7.43) nm.

Copper (II) bacteriochlorin 13^1-(2-sulfoethyl)amide dipotassium salt (12). Bacteriochlorin amide **11** (50 mg) and copper (II) acetate (35 mg) were dissolved in 40 mL of methanol and left under bubbled argon for 10 min. Then, palmitoyl ascorbate (500 mg) was added and the solution was stirred for 30 min. The progress of the reaction was monitored by the spectral shifts of the Q_x and Q_y transitions to 537 and 768 nm, respectively. Next, the reaction mixture was evaporated, redissolved in acetone and filtered to discard excess salt. The acetone was evaporated and the product **12** was purified by HPLC, as described for **5**, using a gradient elution: B, 42% (0 min), 55% (14 min), 100% (16–18 min), 42% (24 min), with a flow rate of 12 mL/min from 0 to 14 min, then 6 mL/min. The purified compound was dried under reduced pressure, redissolved in methanol and separated by filtration from insoluble material. Yield: 46 mg (85%). ESI-MS (–): 795 (M^--2K) *m/z*. UV-VIS in methanol ($\varepsilon \times 10^4\ M^{-1}\ cm^{-1}$): 768 (7.60), 537 (1.67), 387 (5.40) and 342 (6.00) nm.

Zinc bacteriochlorin 13^1-(2-sulfoethyl)amide dipotassium salt (13). Zinc was incorporated into **11** as previously described (47, 48) with some modifications. Thus, a mixture of bacteriochlorin amide **11** (30 mg) and zinc acetate (100 mg) was heated in 5 mL of acetic acid under argon atmosphere at 110°C for about 1 h. The product that accumulated was monitored following the shift of the Q_x transition to 558 nm. Then the reaction mixture was cooled and evaporated. The final purification was carried out by HPLC as for compound **5**. The solvent was evaporated again and the solid compound was collected and stored under argon in the dark at –20°C. Yield: 24 mg (74%). ESI-MS (–): 834 (M^--K), 818 (M^--2K+Na), 796 (M^--2K+H) *m/z*. UV-VIS in methanol ($\varepsilon \times 10^4\ M^{-1}\ cm^{-1}$): 762 (5.51), 558 (1.43), 390 (3.42) and 355 (4.63) nm.

Manganese (III) bacteriochlorin 13^1-(2-sulfoethyl)amide dipotassium salt (14). Manganese insertion into compound **11** was carried out via transmetalation as previously described (47–49) with some modifications. Thus, bacteriochlorin amide **11** (50 mg) in 10 mL of dimethylformamide (DMF) was heated with cadmium acetate (220 mg) under argon atmosphere at 110°C for about 15 min (Cd-complex formation was monitored in acetone by the shift of the Q_x transition from 519 to 585 nm). Then, the reaction mixture was cooled and evaporated. The dry residue was redissolved in 15 mL of acetone and stirred with manganese (II) chloride to form the Mn(III) product **14**. The product formed was monitored in acetone by the shift of the Q_x and Q_y transition from 585 to 600 nm and from 768 to 828 nm, respectively (49). The acetone was evaporated and the product was purified by HPLC using gradient elution by acetonitrile in water: 10% (0 min), 15% (14 min), 100% (16–18 min), 10% (24 min) at a flow rate of 8 mL/min. The purified pigment was then dried under reduced pressure, redissolved in methanol and separated from the insoluble material by filtration. Next, the solvent was evaporated again and the solid compound was stored under argon in the dark at –20°C. Yield: 42 mg (76%). ESI-MS (+): 832 (M^+-2K+2Na) *m/z*. UV-VIS in methanol ($\varepsilon \times 10^4\ M^{-1}\ cm^{-1}$): 825 (4.61), 588 (1.47), 372 (3.75) and 327 (3.78) nm.

H5V mouse endothelial cells were cultured as monolayers in Dulbecco's modified Eagle's medium (DMEM)/F12 containing 25 m*M* 4-(2-hydroxyl)-1-piperazineethanesulfonic acid (HEPES), pH 7.4, 10% fetal bovine serum (FBS), glutamine (2 m*M*), penicillin (0.06 mg/mL) and streptomycin (0.1 mg/mL) (hereafter referred to as the "Culture Medium"). Cells were grown at 37°C in an 8% CO_2-humidified atmosphere.

The photocytotoxicity of the different sensitizers against H5V cells in cultures was determined after preincubation with increasing concentrations of the compounds in the dark for the times and conditions indicated for the individual experiments. Compounds **3** and **7** were primarily dissolved in DMSO (1% of the final volume); all other compounds were dissolved directly in the culture medium. Unbound sensitizer was removed by washing the cells once with culture medium and the plates were illuminated at room temperature from the bottom ($650\ nm < \lambda < 800\ nm$, 12 J/cm^2). The light source used was a 100W Halogen lamp (Osram, Munich, Germany) equipped with a 4-cm water filter. The cultures were placed in the culture incubator and cell survival was determined 24 h after illumination by a Neutral Red viability assay that was validated against the 3-(4,5-

Table 1. Partition values of different Bchl derivatives described in this manuscript, between *n*-octanol and water

Compound	Octanol/water partition (P)	log P
3	96:4	1.38
5	40:60	−0.18
7	74:26	0.45
8	12:88	−0.86
9	23:77	−0.52
10	39:61	−0.19
11	59:41	0.16
12	40:60	−0.18
13	48:52	−0.03
14	5:95	−1.28

dimtheylthiazol-2-yl)-2,5-diphenyl tetrazolium bromide (MTT) viability assay as previously described (17,50). Three kinds of controls were used: (1) light control, cells illuminated in the absence of sensitizers; (2) dark control, cells treated with sensitizer but kept in the dark; and (3) untreated cells that were kept in the dark.

RESULTS

Polarity and solubility

The low solubility and the subsequent aggregation of Bchl derivatives in aqueous solutions pose major problems in their application as VTP reagents. On increasing the polarity of the new derivatives, we expected to see a significant increase in their hydrophilicity and a marked reduction in the aggregation constants. The first parameter was quantified by means of their partitioning coefficient. Table 1 presents the partition coefficients (P) of the new sensitizers in *n*-octanol:water solutions. It appears that cleavage of the isocyclic ring has a profound effect on the molecule's polarity and solubility. Thus, all products of aminolysis presented relatively high polarity (Table 1) that was also reflected in their good solubility in polar organic solvents such as alcohols (methanol, ethanol), DMF and DMSO and their very poor solubility in less polar solvents such as chloroform, acetone and acetonitrile (data not shown). The high polarity of the open ring sensitizers allows for good solubility in water (or PBS) (up to 40 mg/mL with no precipitation after centrifugation at 17 000 ***g***). The increased solubility of **5** or **10** compared with **7** is evidence of the greater significance of the isocyclic ring cleavage compared with the addition of charged peripheral groups for enhancing the polarity/solubility of the Bchl derivatives. Nevertheless, up to ~4 mg/mL of **7** could be introduced into aqueous solutions (*e.g.* PBS) with no precipitation of aggregates upon centrifugation. Because of its amphiphilic nature, **7** could also be introduced into solvents of low polarity like chloroform after dissolving in alcohol (methanol, ethanol) and mixing to make a final alcohol concentration of 3–5%. The addition of a second and even third sulfonic group (**8** and **9**) to the aminolysis products had some effect on P (somewhat enhanced water solubility), whereas metal replacement had a smaller effect as long as the metal redox state was not changed. However, the replacement of Pd(II) by Mn(III) strongly affected P (Table 1). In contrast, changing the length (and thereby the hydrophobicity) of the alkenyl linkage (**5** and **10**) had only a minor effect on P.

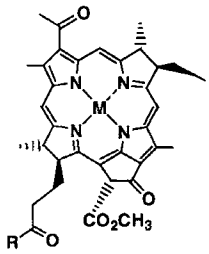

1: M=Mg, R=phytyl
2: M=2H, R=OH
3: M=Pd, R=OH (WST09, Tookad®)
6: M=Pd, R=O-succinimide-$SO_3^-Na^+$
7: M=Pd, R=NH-$(CH_2)_3$-$SO_3^-Na^+$

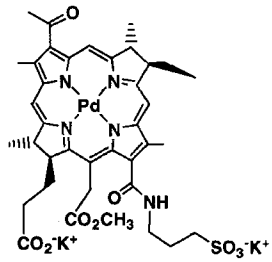

5

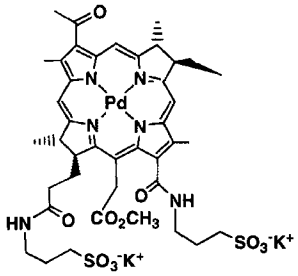

8

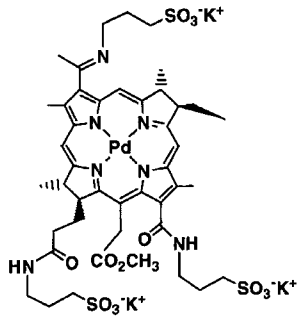

9

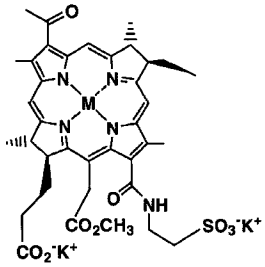

10: M=Pd
11: M=2H
12: M=Cu^{II}
13: M=Zn
14: M=Mn^{III}

Scheme.

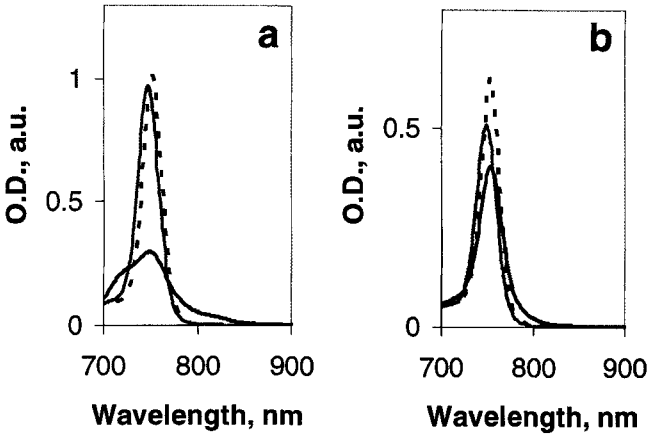

Figure 1. Absorption spectra of Bchl derivatives **10** (a) and **13** (b) (40 μ*M* solutions) in PBS (black), 1% TX-100/PBS (dashed) and methanol (gray). Spectra were recorded with a 2-mm quartz cuvette using a Cary-5E spectrophotometer.

Notably, despite their relatively high solubility, all open-ring products formed small aggregates (estimated to be two to eight molecules; see below and also F. Martinic, Negma-Lerads, private communication) in the aqueous solutions that underwent dissociation upon dilution, micelle incorporation or introduction of physiologic concentrations of serum albumin.

To quantify the aggregation tendency of the different compounds, we first explored the effect of concentration and detergents on their optical absorption and circular dichroism (CD) in serum-free aqueous solutions. Then, we investigated the effect of whole serum on the aggregated state. Next, we examined the affinity of representative compounds to specific serum proteins using size-exclusion chromatography. Finally, we quantified these interactions for BSA by monitoring the effect of BSA on the optical absorption and CD of the selected compound. By employing factor analysis to the resulting spectra, we derived the percentage of monomers, dimers and larger aggregates at a specific total concentration of the selected compound.

Aggregate formation in serum-free solutions

Figure 1 describes the optical absorption of aminolysis products **8**, **10–14** at 40 μ*M* in PBS (black lines) and in methanol (gray lines). The Q_y bands of compounds **8**, **10** and **12** were markedly broadened and attenuated in PBS compared with methanol (Fig. 1a illustrates the absorption spectra of **10**), those of **11** and **13** were less attenuated and slightly broadened (Fig. 1b illustrates the absorption spectra of **13**), whereas the Q_y line shape of **14** hardly changed. Remarkably, the decrease in the extinction coefficients of **8**, **10** and **12** in PBS was accompanied by an overall decrease of the Q_y integrated optical absorption (700–900 nm), suggesting both shading and intensity borrowing by higher electronic transitions because of strong excitonic coupling in the aggregated states, as previously found for Bchl *a* and Chl *a* (51–53).

The effect of concentration. The effect of concentration on the optical absorption and CD spectra of the aminolysis products in PBS is illustrated for **10** in Fig. 2a,b, respectively. The presented spectra were recorded using quartz cuvettes with different path lengths (l) and then multiplied by ($l_x/l_{40} \cdot 40/X$), where X stands for the recorded concentration. Notably, on increasing the concentration, the monomeric Q_y transition at ~750 nm split into new

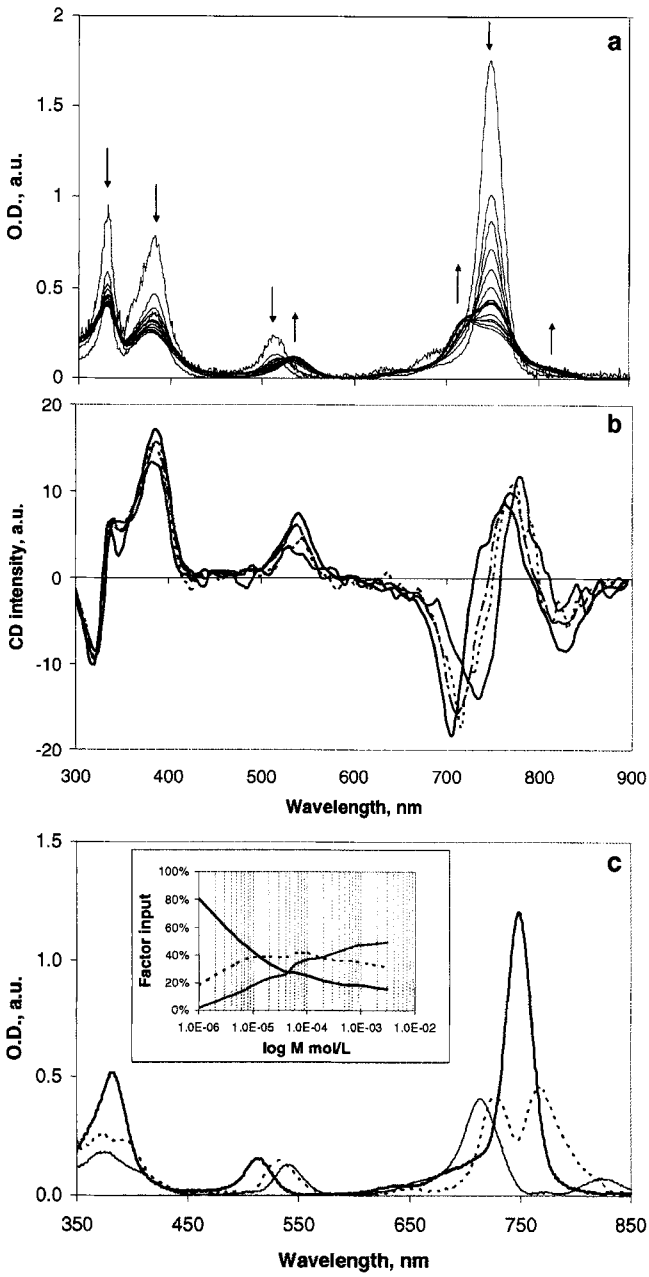

Figure 2. The effect of concentration on the spectra of compound **10**. a: The optical absorption of **10** at 0.1 μ*M* to 3 m*M*. Spectra were recorded using different optical path-lengths (l) and then multiplied by ($l_x/l_{40} \cdot 40/X$), where X stands for the recorded concentration (μ*M*); arrows indicate changes upon increasing the concentration of **10**. b: The circular dichroism spectra of selected concentrations of **10** in PBS solution (the spectra normalized as described above): 10 μ*M* (gray line), 80 μ*M* (dotted line), 200 μ*M* (dashed–dotted line) and 3 m*M* (solid line). c: Principal components of the optical absorption resolved by factor analysis: Solid line, monomer; dashed line, dimer; gray line, larger aggregate (probably hexamer or octamer). Inset: The dependence of the principal components on the concentration of **10**.

electronic transitions at higher and lower energies, as expected upon the formation of excitonically coupled aggregates.

Using the previously described factor analysis technique (44), we found three spectroscopic components that accounted for the spectroscopic evolution throughout the entire concentration range (Fig. 2c). The first component (solid line) has a spectrum similar to that of **10** in methanol, with a slightly broadened Q_y transition (at

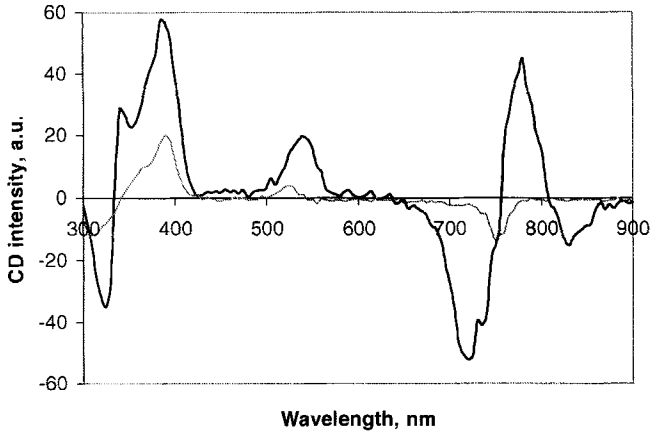

Figure 3. CD spectra of compound **10** (40 μ*M*, in 5- and 10-mm quartz cuvettes using an Aviv-202 CD spectrometer) in PBS (black line) and 1% TX-100/PBS (gray line).

750 nm). Hence, this spectrum is assigned to monomers. In the second component (dotted line), the Q_y transition splits into two new excitonic transitions at 726 and 765 nm. In the third component (gray line), the energy difference between the upper and lower excitonic transitions (712 and 822 nm, respectively) is markedly increased. Assuming that the exciton splitting reflects the extent of coupling among the individual transition dipoles (51–56), the concentration dependence of the **10** in the spectra clearly indicates the formation of two forms of aggregates: small ones, probably dimers (Fig. 2c, dashed line) with strong excitonic splitting ($\Delta\nu$ ~750 cm^{-1}) among two major transition dipoles and at increasing concentrations of **10** and larger ones consisting of at least hexamers (Fig. 2c, gray line), with increased splitting (1900 cm^{-1}) but similar coupling among the Q_y transition dipoles.

The CD spectra (Fig. 2b) provide complementary evidence to the factor analyses' assignments being dominated by different excitonically coupled components, at the intermediate (negative and positive bands at 735 and 780 nm, respectively) and high (negative, positive, and negative bands at 705, 765 and 825 nm, respectively) concentration ranges. The contribution of the monomeric species (weak negative band at 750 nm, identified by recording solutions of **10** in PBS/Triton X-100 [TX-100]) (Fig. 3) becomes apparent at a very low concentration. Importantly, the CD spectra of the two lowest concentrations are not shown because of too low signal/noise values.

The relative contributions of the principal components (Fig. 2c, inset) provided the means for calculating the monomer/dimer equilibrium at low concentrations of **10**, where the higher oligomer contribution is negligible (inset, left side, Fig. 2c):

$$2 \cdot \mathbf{10} \Longleftrightarrow (\mathbf{10})_2$$

$$K_{\text{dimerization}} = [(\mathbf{10})_2]/[\mathbf{10}]^2$$

Substituting $0.8 \cdot 10^{-6}$ and $0.2 \cdot 10^{-6}$ for [**10**] and [$(\mathbf{10})_2$], respectively (based on the contributions of the principal components presented in the inset, Fig. 2c), we obtain

$$K_{\text{dimerization}} = 3 \cdot 10^5\ M^{-1}.$$

The effect of detergents. In our previous studies of Bchl and Chl aggregation in different solvents, we found that the addition of TX-100 to aqueous solutions of Bchl/Chl induced disaggregation into monomers trapped in the formed TX-100 micelles (51–56). Following this observation, we tested the effect of adding TX-100, above the critical micelle concentration (53, 55), to the presently examined derivatives of Bchl (Fig. 1, dashed lines). Indeed, the line shape and peak position of the Q_y transition of all tested compounds (~825 for Mn derivative **14** and ~750–760 nm for the other compounds) in PBS/TX-100 appeared similar to the monomeric spectra in methanol, with a single negative Cotton effect at the peak of the Q_y transition, as illustrated for **10** (Fig. 3). Notably, the Mn complex **14** appeared practically monomeric in aqueous solution, both in the absence or presence of TX-100 micelles. The metal-free **11** and Zn complex **13** form loose aggregates (probably dimers) with relatively small excitonic splitting (Fig. 1b), whereas in Pd compounds **8** and **10** and in Cu complex **12**, these small aggregates appeared to assemble into larger ones with strong interactions among their transition dipoles (Fig. 1a).

Aggregate formation in serum/PBS solutions: the effect of serum proteins

The opening of the isocyclic ring by aminolysis appeared to have a dramatic effect on the hydrophobicity of the compounds, as reflected by their aggregation in aqueous solutions (Fig. 1). Consequently, these compounds should become more amenable to solvation by serum proteins. Thus, when FCS was added to **3** (Tookad®) or **7**, the compounds with intact isocyclic rings, the Q_y transition remained broad and redshifted to 800–830 nm, as expected for high-aggregate content (Fig. 4a,b, respectively). In contrast, upon adding FCS or BSA to **10**, as with all other products of aminolysis in aqueous solutions, the line shape of the Q_y transitions became monomeric, similar to that observed in organic solvent (Fig. 4c).

Considering **3** and **10** as representatives of hydrophobic and hydrophilic Bchl derivatives, respectively, we set out to resolve their interactions with specific serum proteins.

Binding compounds 3 and 10 to lipoproteins and serum albumin, respectively

Figure 5a–c describes the elution profiles of the major proteins in FCS, the protein-associated **3** (Tookad®) and the protein-associated **10** (WST11), respectively, after being mixed with FCS as described in Materials and Methods. Remarkably, a significant portion of **3** was eluted with the void volume, probably in the form of very large aggregates (having a maximum absorption at 825 nm). The protein-associated **3** (optical absorption at 760 nm) mainly comprised HDL (>90%) and a minor fraction was found associated with the serum albumin component (Fig. 5b). Considering the relative concentrations of serum albumin and HDL in the plasma, the affinity of **3** to serum albumin should be negligible compared with HDL. In contrast, **10** mostly adsorbed to serum albumin (Fig. 5c), with a minor fraction being eluted with the lipoproteins.

To determine the association constant of **10** and BSA, we resolved the concentrations of the protein complex [**10**-BSA] and the corresponding monomer concentrations [**10**] using two experimental approaches: (1) chromatographically, by measuring the [**10**-BSA] values after chromatographic separation of the protein-associated compound in different mixtures of **10** and BSA and (2) spectroscopically, by deriving the monomeric optical absorption using factor analysis, in solutions of **10** with different concentrations of BSA.

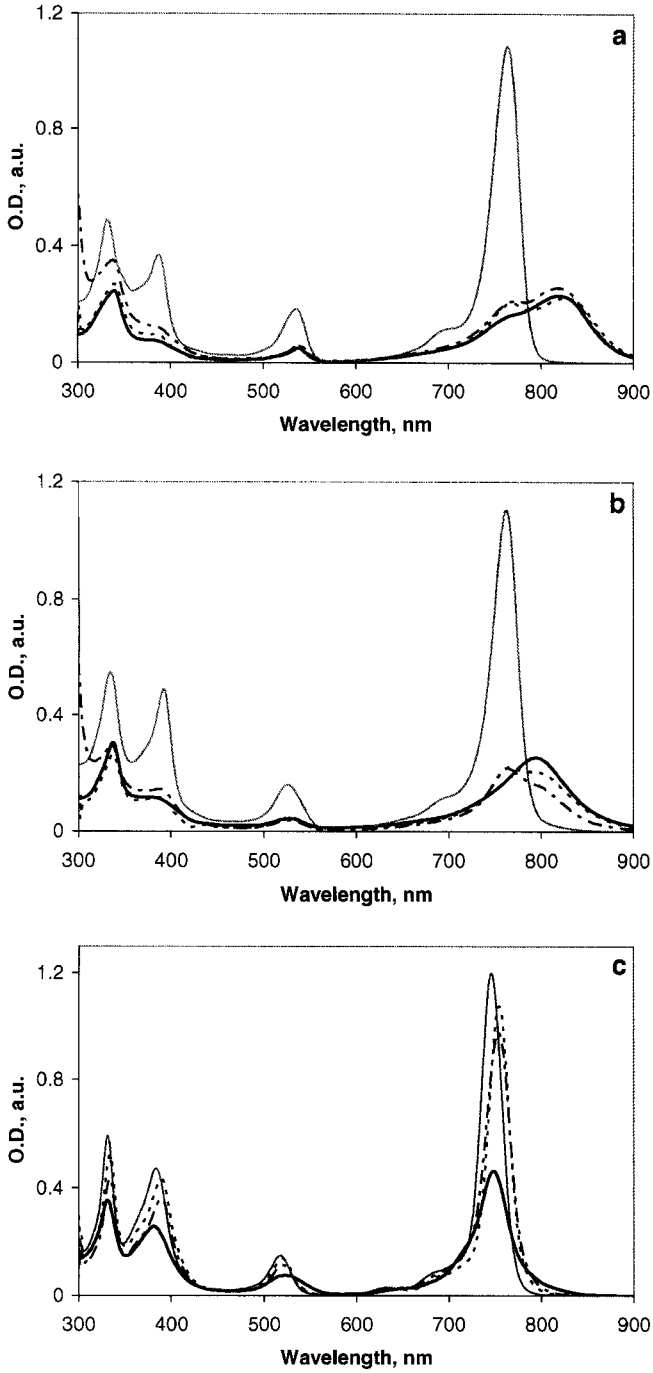

Figure 4. The effect of diluting different Bchl derivative in PBS by solutions of FCS or BSA to make a final sensitizer's concentration of 10 μ*M*, on their optical absorption (recorded in 10-mm quartz cuvettes). a: Compound **3** (obtained by dilution of 2.5 mg/mL Tookad® solution stabilized with Cremophor EL®). b: Compound **7** (initially dissolved in PBS). c: Compound **10** (initially dissolved in PBS). Solid black line, spectra in PBS; dotted line, in 90% FCS/PBS; dashed–dotted line, in 540 μ*M* BSA/PBS; solid gray line, in organic solvent (chloroform for **3**, chloroform/methanol [90:10] for **7** and methanol for **10**).

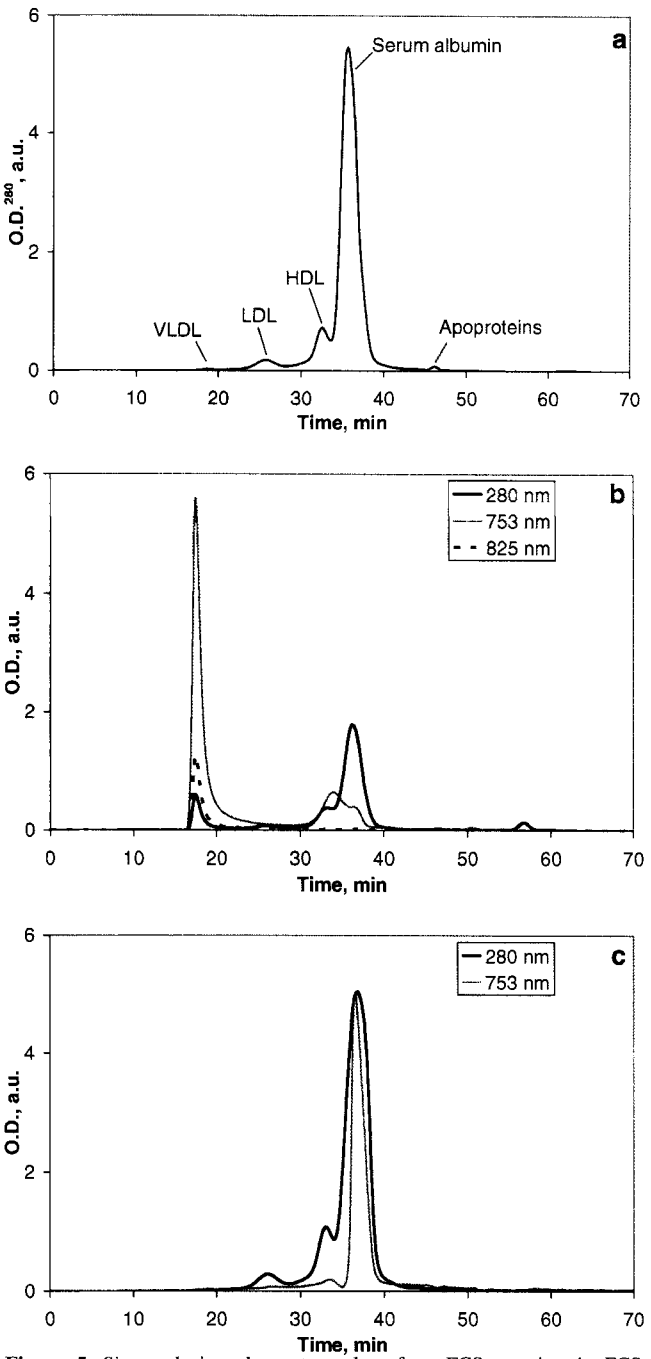

Figure 5. Size-exclusion chromatography of: a, FCS proteins. b, FCS protein-associated **3** (Tookad®) and c, FCS protein-associated **10** (WST11). The chromatogram profiles in b and c are normalized for better viewing.

Chromatographic determination of [10-BSA]. Table 2 presents the concentrations of **10** and BSA after mixing 10 μ*M* BSA with different concentrations of **10** in PBS followed by flash separation with size exclusion.

Assuming a simple, second-order equation:

$$\mathbf{10} + \mathrm{BSA} \Longleftrightarrow \mathbf{10} - \mathrm{BSA};$$

$$K_{\mathrm{assoc}} = \frac{[\mathbf{10} \cdot BSA]}{[\mathbf{10}] \cdot [BSA]}.$$

The average value of K_{assoc} amounts to $\sim 10^4\ M^{-1}$.

Determination of [10-BSA] values at different concentrations of BSA and 40 μM 10 using factor analysis of the corresponding optical absorption spectra. Figure 6a,b illustrates the optical absorption and CD spectra, respectively, of 40 μ*M* **10** in the presence of different BSA concentrations. Using factor analysis for the optical absorption spectra as previously described, we were

Table 2. The concentration of free ([**10**]) and BSA-bound ([**10**-BSA]) WST11 after mixing 50 μ*M* WST11 with 10 μ*M* BSA

Experiment no.	[**10**] × 10^{-6} *M*	[BSA] × 10^{-6} *M*	[**10**-BSA] × 10^{-6} *M*	$K_{assoc} \times 10^3$
1	1.87	9.87	0.13	7.0
2	4.53	9.53	0.47	10.9
5	9.00	9.00	1.00	12.3
3	18.67	8.67	1.33	8.2
4	47.10	7.10	2.90	8.7

able to resolve the concentrations of three principal components (Fig. 6a, inset) that appear similar to monomeric (solid line), dimeric (dashed line) and higher-order aggregates (gray line). The line shape of these components is also similar to those resolved for different concentrations of **10** in the absence of BSA. Using the relative contribution of the different components and the overall concentration of **10**, we arrived at an association constant of $K_{assoc} = 1 \cdot 10^4\ M^{-1}$, assuming that **10**-BSA comprises only bound monomers. Thus both methods, chromatographic and spectroscopic, provided similar results. The construction of a physical model that includes the detailed equilibrium constants between the different aggregates is in progress. Using the obtained association constant between BSA and **10**, one expects that at physiologic concentrations of BSA (~0.6 m*M*) about 2 μ*M* **10** (5%) remains nonbound to BSA.

Photocytotoxicity of the new compounds in the absence and presence of serum proteins

The phototoxicity of compounds **3** and **7–14** was tested on cultured H5V mouse endothelial cells by two experimental procedures. In the first procedure, after our previous experiments (21,50,57), cells were preincubated in the presence of 10% FCS with increasing concentrations of the test compounds for 2 h, then washed and illuminated or kept in the dark. The second procedure attempted to simulate the conditions of *in vivo* VTP, where illumination is applied immediately after intravenous administration of the test compound (sensitizer) in the presence of physiologic concentrations of serum proteins and decreasing concentrations of the sensitizer in the plasma (because of rapid clearance [25,38]). Within the illumination time (5–10 min, immediately after administrating bolus sensitizer) the plasma concentrations of all currently tested sensitizers decreased to less than 5% of their initial values (*e.g.* 38,58). Hence, the average sensitizer concentration during illumination is ~$[C_0]/2$, where $[C_0]$ is the initial concentration of the sensitizer in the plasma, usually in the range of 100 μ*M* (in the blood). Following these constraints, in testing the second procedure in the present study, we applied a 10-min illumination after a 3-min incubation of the different compounds (50 μ*M*) with endothelial cells in the presence of 0–75% FCS or 0–540 μ*M* BSA without washing.

The results of the first procedure are presented in Table 3. The phototoxicities of compounds **8** and **10** were concentration- and light-dependent, without substantial dark toxicity in the tested range. The LD_{50} of the nonmetalated compound **11** and the Pd-containing sensitizers **3**, **5**, **7–10** were almost the same (~1–5 μ*M*), whereas the complexes with Cu, Zn and Mn (**12–14**) were photodynamically inactive (the Zn complex was found inoperative due to its oxidation into chlorin during 2 h incubation).

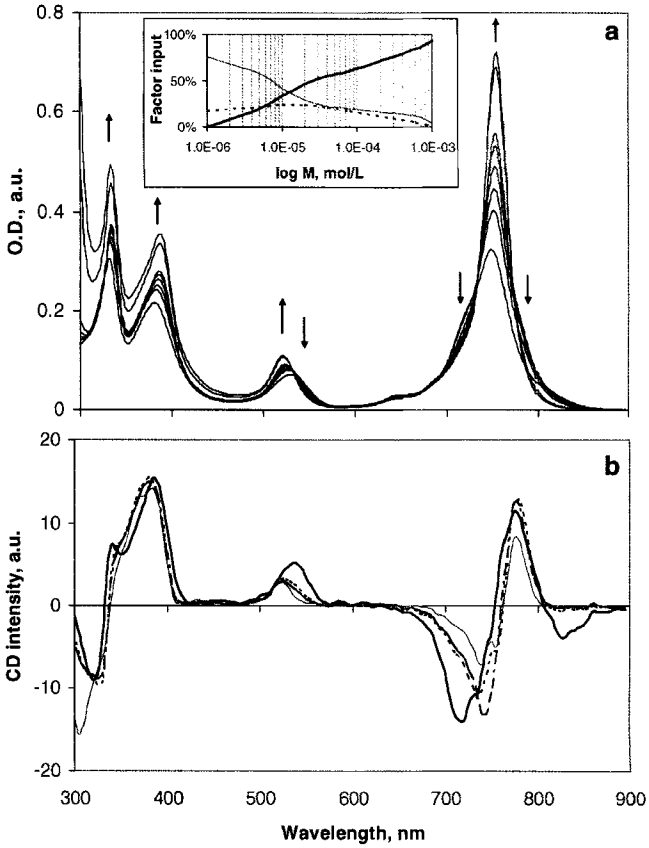

Figure 6. Aggregation forms of **10** in PBS at a constant pigment concentration (40 μ*M*) and increasing concentrations of BSA (0–1 m*M*). a: Absorption spectra (spectra were recorded and normalized as described in the legend for Fig. 2a); arrows indicate changes upon an increase in BSA concentration. Inset: Dependence of the principal components of the optical absorption on the concentration of BSA as resolved by factor analysis of the optical absorption. Solid line, monomer; dashed line, dimer; gray line, oligomer. b: CD spectra (spectra were recorded and normalized as described in the legend for Fig. 2a): no BSA, solid black line; 40 μ*M*, dotted line; 80 μ*M*, dashed–dotted line; 1 m*M*, gray solid line.

The results of the second procedure are displayed in Fig. 7. Evidently, the photocytotoxicity of the palladium-containing compounds **7–10** and the zinc complex **13** declined markedly, whereas that of **3** (Tookad®) and the metal-free **11** remained the same (Fig. 7a). Derivatives with copper **12** and manganese **14** were photoinactive at all serum concentrations examined. Similar results were obtained when BSA was used instead of whole serum (Fig. 7b).

Based on the synthetic simplicity and the near resemblance of physicochemical properties of Pd complexes **5**, **8** and **10**, the latter taurinated* compound was chosen as the main representative of water-soluble Bchl derivatives for further biological examination (24,38). This compound was found to be stable in solutions (in contrast to the zinc derivative **13**; data not shown) as well as during prolonged storage (months), when kept as a solid in the dark at –20°C.

*Taurine (2-amino-1-ethane sulfonic acid), a close homologue of homotaurine, is a widely available biochemical product. Taurine is not poisonous; on the contrary, it is a conditionally essential nutrient, important for mammalian development, especially for cerebellum and retina cells (59); for the biological and therapeutic potential of taurine, see reviews (60–62).

Table 3. Sensitizers' phototoxicity. H5V cells were preincubated with compounds **3** and **7–14** in medium containing 10% FCS for 2 h, then washed with fresh medium and illuminated. Points are the mean ± SEM of triplicate determinations

Compound no.	LD_{50} (μM)
3	1.0
5	2.1
7	3.1
8	1.5
9	5.2
10	0.8
11	1.8
12	n.d.*
13	n.d.
14	n.d.

*n.d., nondetected.

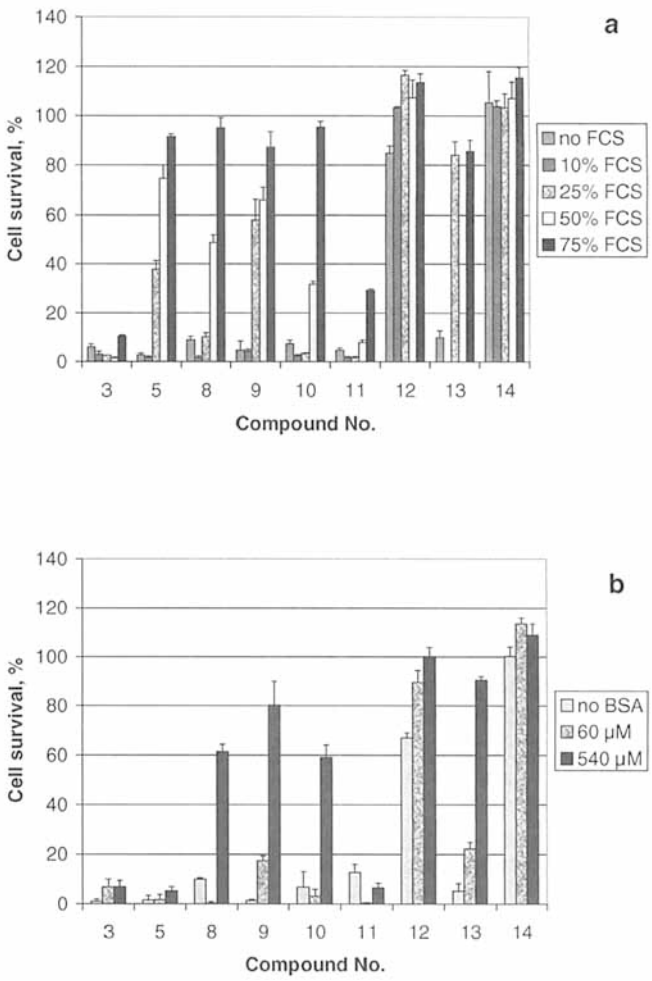

Figure 7. Phototoxicity dependence on the concentration of serum (a) and BSA (b). H5V cells were preincubated with 50 μM concentrations of the indicated pigments in cell culture medium for 3 min, illuminated for 10 min, then washed with fresh medium. The points are the mean ± SEM of triplicate determinations.

DISCUSSION AND CONCLUSIONS

Preclinical and clinical trials with antiangiogenic agents have been at the cutting edge of tumor therapy for quite some time. However, systemic application of antiangiogenic agents, which prevents the development of new blood vessels and thereby inhibits tumor growth, was found most effective in regions of neovascularization such as the tumor periphery, but not in areas of existing tumors with a supply of mature vessels or in tumor regions that share vascularization with adjacent normal tissues (63,64). Vascular targeting agents (VTA) provide an interesting alternative, but such agents were found more active in the interior of relatively large tumors, possibly because of the high interstitial pressure in these regions, which contributes to vascular collapse (64). Furthermore, VTA often generate a characteristic pattern of widespread central necrosis in experimental tumors, which can extend to as much as 95% of the tumor volume. However, a thin frame of tumor cells at the tumor's rim may survive, resulting in tumor regrowth. Thus, despite very promising experimental results, both antiangiogenic and antivascular targeting agents have so far failed in completely eradicating tumors. VTA and therapies designed for direct tumor cell killing (conventional chemotherapeutic drugs, radiation or PDT based on cell-selective uptake) are awaiting further development (64–66).

Recent promising results with VTP therapy based on a Bchl derivative to achieve complete tumor eradication showed high cure rates with various tumor types (20,58,67). In the present study we focused on the synthesis and characterization of new Bchl-type candidates for VTP. Here we showed that aminolysis of the isocyclic ring with negatively charged residues markedly increases the hydrophilicity of the Bchl sensitizers, decreases their self-association constant and selectively increases their affinity to serum albumin, compared with other serum proteins. To that end, we suggest several simple analytical procedures that can be applied to other sensitizers as well. The remarkable polarity and solubility of compound **14**, compared with the other products of Bpheid aminolysis, probably reflects the high dipole moment of this molecule. As we have recently shown (49), the Mn(III)Bpheid derivatives are axially biligated with hydroxyl anion and hydroperoxide in the absence of other strong ligands.

The enhanced hydrophilicity and increased affinity of some of the new sensitizers to serum albumin seem advantageous for VTP. This is mainly because serum albumin stays in the circulation and can also bring the sensitizers to the vasculature of important target organs, such as the liver and lungs, as recently shown for the biodistribution of compound **10** (38). However, the concomitant reduction in the photocytotoxicity toward endothelial cells appears at first to be a drawback for this treatment modality because a direct insult of endothelial cells is considered important for successfully launching a tumor cure via VTP (12). Strikingly, in several studies that were recently performed in our laboratory (24,38; Mazor *et al.*, unpublished data), we showed that such sensitizers are highly efficacious VTP agents that deliver high cure rates for a variety of tumor types. However, these experiments showed that, unlike Tookad®, VTP with **10** has practically no effect on the vessels' permeability. Thus, the occlusion of tumor vessels, which was observed within minutes of illumination, was not accompanied by hemorrhagic necrosis, underscoring the advantage of such sensitizers for VTP applications where hemorrhagic necrosis may endanger the treated patient, such as in tumors situated near major vessels or in internal sensitive organs or in age-related macular degeneration, in which lateral photodamage may be considerable.

Acknowledgements—This study was supported by grants from the Yeda Research and Development Co., Ltd. (Israel) and Steba-Biotech (France).

We are grateful to Dr. Vlad Brumfeld for his assistance in circular dichroism spectroscopy and to Dr. Roie Yerushalmi for factor analysis. A.S. is the incumbent of the Robert and Yadelle Sklare Professorial Chair in Biochemistry. Y.S. is the incumbent of the Tillie and Charles Lubin Professorial Chair in Biochemical Endocrinology.

REFERENCES

1. Folkman, J. (1995) Angiogenesis in cancer, vascular, rheumatoid and other disease. *Nat. Med.* **1**, 27–31.
2. Schnitzer, J. E. (1998) Vascular targeting as a strategy for cancer therapy. *N. Engl. J. Med.* **339**, 472–474.
3. Paris, F., Z. Fuks, A. Kang, P. Capodieci, G. Juan, D. Ehleiter, A. Haimovitz-Friedman, C. Cordon-Cardo and R. Kolesnick (2001) Endothelial apoptosis as the primary lesion initiating intestinal radiation damage in mice. *Science* **293**(5528), 293–297.
4. Molema, G. (2002) Tumor vasculature directed drug targeting: applying new technologies and knowledge to the development of clinically relevant therapies. *Pharm. Res.* **19**, 1251–1258.
5. Miller, J. W. (2003) Photodynamic therapy for choroidal neovascularization. *Graefe's Arch. Clin. Exp. Ophthalmol.* **241**, 258–262.
6. Rupnick, M. A., D. Panigrahy, C. Y. Zhang, S. M. Dallabrida, B. B. Lowell, R. Langer and M. J. Folkman (2002) Adipose tissue mass can be regulated through the vasculature. *Proc. Natl. Acad. Sci. USA* **99**, 10730–10735.
7. Renno, R. Z. and J. W. Miller (2001) Photosensitizer delivery for photodynamic therapy of choroidal neovascularization. *Adv. Drug Deliv. Rev.* **52**, 63–78.
8. Boyle, R. W. and D. Dolphin (1996) Structure and biodistribution relationships of photodynamic sensitizers. *Photochem. Photobiol.* **64**, 469–485.
9. Dougherty, T. J., C. J. Gomer, B. W. Henderson, G. Jori, D. Kessel, M. Korbelik, J. Moan and Q. Peng (1998) Photodynamic therapy. *J. Natl. Cancer Inst.* **90**, 889–905.
10. Pandey, R. K. and G. Zheng (2000) Porphyrins as photosensitizers in photodynamic therapy. In *The Porphyrin Handbook*, Vol. 6 (Edited by K. M. Kadish, K. M. Smith and R. Guilard), pp. 157–230. Academic Press, San Diego.
11. Macdonald, I. J. and T. J. Dougherty (2001) Basic principles of photodynamic therapy. *J. Porphyrins Phthalocyanines* **5**, 105–129.
12. Abels, C. (2004) Targeting of the vascular system of solid tumours by photodynamic therapy (PDT). *Photochem. Photobiol. Sci.* **3**, 765–771.
13. Krammer, B. (2001) Vascular effects of photodynamic therapy. *Anticancer Res.* **21**, 4271–4277.
14. Ferrario, A., D. Kessel and C. J. Gomer (1992) Metabolic properties and photosensitizing responsiveness of mono-L-aspartyl chlorin-e6 in a mouse-tumor model. *Cancer Res.* **52**, 2890–2893.
15. Roberts, W. G. and T. Hasan (1992) Role of neovasculature and vascular-permeability on the tumor retention of photodynamic agents. *Cancer Res.* **52**, 924–930.
16. McMahon, K. S., T. J. Wieman, P. H. Moore and V. H. Fingar (1994) Effects of photodynamic therapy using mono-L-aspartyl chlorin E(6) on vessel constriction, vessel leakage, and tumor response. *Cancer Res.* **54**, 5374–5379.
17. Zilberstein, J., S. Schreiber, M. C. W. M. Bloemers, P. Bendel, M. Neeman, E. Schechtman, F. Kohen, A. Scherz and Y. Salomon (2001) Antivascular treatment of solid melanoma tumors with bacteriochlorophyll-serine-based photodynamic therapy. *Photochem. Photobiol.* **73**, 257–266.
18. Dolmans, D. E. J. G. J., A. Kadambi, J. S. Hill, K. R. Flores, J. N. Gerber, J. P. Walker, I. H. M. Borel Rinkes, R. K. Jain and D. Fukumura (2002) Targeting tumor vasculature and cancer cells in orthotopic breast tumor by fractionated photosensitizer dosing photodynamic therapy. *Cancer Res.* **62**, 4289–4294.
19. Gross, S., A. Gilead, O. Mazor, A. Brandis, S. Schreiber, Y. Machluf, M. Neeman, A. Scherz and Y. Salomon (2003) Selective vascular and tumor responses to photodynamic therapy (PDT) with Pd bacteriopheophorbide (TOOKAD): online and offline analyses. *Proc. Am. Assoc. Cancer Res.* **44**, 27.
20. Koudinova, N. V., J. H. Pinthus, A. Brandis, O. Brenner, P. Bendel, J. Ramon, Z. Eshhar, A. Scherz and Y. Salomon (2003) Photodynamic therapy with Pd-bacteriopheophorbide (TOOKAD): successful *in vivo* treatment of human prostatic small cell carcinoma xenografts. *Int. J. Cancer* **104**, 782–789.
21. Preise, D., O. Mazor, N. Koudinova, M. Liskovich, A. Scherz and Y. Salomon (2003) Bypass of tumor drug resistance by antivascular therapy. *Neoplasia* **5**, 475–480.
22. Kelleher, D. K., O. Thews, A. Scherz, Y. Salomon and P. Vaupel (2004) Perfusion, oxygenation status and growth of experimental tumors upon photodynamic therapy with Pd-bacteriopheophorbide. *Int. J. Oncol.* **24**, 1505–1511.
23. Scherz, A., Y. Salomon, A. Brandis and H. Scheer (2003) Palladium-substituted Bacteriochlorophyll Derivatives and Use Thereof. U.S. Patent 6 569 846.
24. Mazor, O. (2004) Synthesis and Phototoxicity of Novel Sulfonated Bacteriochlorophyll Derivatives. Ph.D. thesis, Weizmann Institute of Science, Rehovot, Israel.
25. Brun, P. H., J. L. DeGroot, E. F. G. Dickson, M. Farahari and R. H. Pottier (2004) Determination of the in vivo pharmacokinetics of palladium-bacteriopheophorbide (WST09) in EMT6 tumour-bearing Balb/c mice using graphite furnace atomic absorption spectroscopy. *Photochem. Photobiol. Sci.* **3**, 1006–1010.
26. Chen, Y., G. Li and R. K. Pandey (2004) Synthesis of bacteriochlorins and their potential utility in photodynamic therapy (PDT). *Curr. Org. Chem.* **8**, 1105–1134.
27. Shargel, L. and A. B. C. Yu (1999) *Applied Biopharmaceutics and Pharmacokinetics*. Appleton & Lange, McGraw-Hill, New York.
28. Borle, F., A. Radu, C. Fontolliet, H. van den Bergh, P. Monnier and G. Wagnieres (2003) Selectivity of the photosensitiser Tookad® for photodynamic therapy evaluated in the Syrian golden hamster cheek pouch tumour model. *Br. J. Cancer* **89**, 2320.
29. Chen, Q., Z. Huang, D. Luck, J. Beckers, P.-H. Brun, B. C. Wilson, A. Scherz, Y. Salomon and F. Hetzel (2002) Preclinical studies in normal canine prostate of a novel palladium-bacteriopheophorbide (WST09) photosensitizer for photodynamic therapy of prostate cancer. *Photochem. Photobiol.* **76**, 438–445.
30. Weller, A. and R. Livingstone (1954) The reaction of chlorophyll in amines. *J. Am. Chem. Soc.* **76**, 1575–1578.
31. Pennington, F. C., S. D. Boyd, H. Horton, S. W. Taylor, D. G. Wulf, J. J. Katz and H. H. Strain (1967) Reactions of chlorophylls a and b with amines. Isocyclic ring rupture and formation of substituted chlorin-6-amides. *J. Am. Chem. Soc.* **89**, 3871–3875.
32. Ando, T., K. Irie, K. Koshimizu, T. Shingu, N. Takeda, T. Takemura, S. Nakajima and I. Sakata (1991) New photosensitizers for photodynamic therapy: syntheses of chlorin e6 dimer and trimer. *Agric. Biol. Chem.* **55**, 2441–2443.
33. Ando, T., I. Kazuhiro, K. Koshimizu, S. Nakajima, T. Takemura and I. Sakata (1992) A convenient synthesis of chlorin e6 dimer and trimer. In *Photodynamic Therapy and Biomedical Lasers* (Edited by P. Spinelli, M. Dal Fante and R. Marchesini), pp. 769–773. Elsevier Science Publishers B.V., Amsterdam.
34. Gurinovich, G. P., T. E. Zorina, S. B. Melnov, N. I. Melnova, I. F. Gurinovich, L. A. Grubina, M. V. Sarzhevskaya and S. N. Cherenkevich (1992) Photodynamic activity of chlorin e_6 and chlorin e_6 ethylenediamide *in vitro* and *in vivo*. *J. Photochem. Photobiol. B Biol.* **13**, 51–57.
35. Ma, L. F. and D. Dolphin (1996) Nucleophilic reaction of 1,8-diazabicyclo[5.4.0]undec-7-ene and 1,5-diazabicyclo[4.3.0]non-5-ene with methyl pheophorbide *a*. Unexpected products. *Tetrahedron* **52**, 849–860.
36. Zhang, L. and D. Y. Xu (1999) Synthesis of chlorin e(6)-6-amide derivatives. *Chin. J. Org. Chem.* **19**, 424–430.
37. Belykh, D. V., L. P. Karmanova, L. V. Spirikhin and A. V. Kutchin (2002) Synthesis of chlorin e_6 amide derivatives. *Mendeleev Commun.* 77–78.
38. Mazor, O., A. Brandis, V. Plaks, V. Rosenbach-Belkin, Y. Salomon and A. Scherz (2005) WST11, a novel water-soluble bacteriochlorophyll derivative; cellular uptake, pharmacokinetics, biodistribution, and vascular targeted photodynamic activity against melanoma tumors. *Photochem. Photobiol.* **81**, 342–351.
39. Gross, S., A. Brandis, L. Chen, V. Rosenbach-Belkin, S. Roehrs, A. Scherz and Y. Salomon (1997) Protein-A-mediated targeting of bacteriochlorophyll-IgG to *Staphylococcus aureus*: a model for enhanced site-specific photocytotoxicity. *Photochem. Photobiol.* **66**, 872–878.
40. Kessel, D. (1989) Determinants of photosensitization by mono-L-aspartyl chlorin e6. *Photochem. Photobiol.* **49**, 447–452.

41. Westerlund, J. and Z. Yao (1995) Elution of lipoprotein fractions containing apolipoproteins E and A-I in size exclusion on Superose 6 columns is sensitive to mobile phase pH and ionic strength. *J. Chromatogr. A* **718**, 59–66.
42. Ordovas, J. M. and D. Osgood (1998) Preparative isolation of plasma lipoproteins using fast protein liquid chromatography. In *Lipoprotein Protocols*, Vol. 110 (Edited by J. Ordovas), pp. 105–111. Humana Press, Inc., Totowa, NJ.
43. Havel, R. J., H. A. Eder and J. H. Bragdon (1955) The distribution and chemical composition of ultracentrifugally separated lipoprotein in human sera. *J. Clin. Investig.* **34**, 1345–1353.
44. Noy, D., R. Yerushalmi, V. Brumfeld, I. Ashur, H. Scheer, K. Baldridge and A. Scherz (2000) Optical absorption and computational studies of [Ni]-bacteriochlorophyll-a. New insight into charge distribution between metal and ligands. *J. Am. Chem. Soc.* **122**, 3937–3944.
45. Wasielewski, M. R. and W. A. Svec (1980) Synthesis of covalently linked dimeric derivatives of chlorophyll a, pyrochlorophyll a, chlorophyll b, and bacteriochlorophyll a. *J. Org. Chem.* **45**, 1969–1974.
46. Scherz, A., L. Fiedor and Y. Salomon (1998) Chlorophyll and Bacteriochlorophyll Derivatives, Their Preparation and Pharmaceutical Compositions Comprising Them. U.S. Patent 5 726 169.
47. Scherz, A., Y. Salomon, H. Scheer, G. Hartwich and A. Brandis (2001) Synthetic Metal-substituted Bacteriochlorophyll Derivatives and Use Thereof. U.S. Patent 6 333 319.
48. Hartwich, G., L. Fiedor, I. Simonin, E. Cmiel, W. Schafer, D. Noy, A. Scherz and H. Scheer (1998) Metal-substituted bacteriochlorophylls. 1. Preparation and influence of metal and coordination on spectra. *J. Am. Chem. Soc.* **120**, 3675–3683.
49. Ashur, I., A. Brandis, M. Greenwald, Y. Vakrat-Haglili, V. Rosenbach-Belkin, H. Scheer and A. Scherz (2003) Control of redox transitions and oxygen species binding in Mn centers by biologically significant ligands; model studies with [Mn]-bacteriochlorophyll a. *J. Am. Chem. Soc.* **125**, 8852–8861.
50. Rosenbach-Belkin, V., L. Chen, L. Fiedor, I. Tregub, F. Pavlotsky, V. Brumfeld, Y. Salomon and A. Scherz (1996) Serine conjugates of chlorophyll and bacteriochlorophyll: photocytotoxicity *in vitro* and tissue distribution in mice bearing melanoma tumors. *Photochem. Photobiol.* **64**, 174–181.
51. Scherz, A. and W. W. Parson (1984) Oligomers of bacteriochlorophyll and bacteriopheophytin with spectroscopic properties resembling those found in photosynthetic bacteria. *Biochim. Biophys. Acta* **766**, 653–665.
52. Scherz, A. and V. Rosenbach-Belkin (1988) The spectral properties of chlorophyll and bacteriochlorophyll dimers; a comparative study. In *NATO ASI Series, Series A: Life Sciences*, Vol. 149 (Photosynth. Bact. React. Cent.), pp. 295–306.
53. Fisher, J. R. E., V. Rosenbach-Belkin and A. Scherz (1990) Cooperative polymerization of photosynthetic pigments in formamide-water solution. *Biophys. J.* **58**, 461–470.
54. Scherz, A. and W. W. Parson (1984) Exciton interactions in dimers of bacteriochlorophyll and related molecules. *Biochim. Biophys. Acta* **766**, 666–678.
55. Scherz, A. and V. Rosenbach-Belkin (1989) Comparative study of optical absorption and circular dichroism of bacteriochlorophyll oligomers in Triton X-100, the antenna pigment B850, and the primary donor P-860 of photosynthetic bacteria indicates that all are similar dimers of bacteriochlorophyll a. *Proc. Natl. Acad. Sci. USA* **86**, 1505–1509.
56. Rosenbach-Belkin, V., J. R. E. Fisher and A. Scherz (1991) Effect of nonexcitonic interactions among the paired molecules on the Qy transition of bacteriochlorophyll dimers. Applications to the primary electron donors P-860 and P-960 in bacterial reaction centers. *J. Am. Chem. Soc.* **113**, 676–678.
57. Plaks, V., Y. Posen, O. Mazor, A. Brandis, A. Scherz and Y. Salomon (2004) Homologous adaptation to oxidative stress induced by the photosensitized Pd-bacteriochlorophyll derivative (WST11) in cultured endothelial cells. *J. Biol. Chem.* **279**, 45713–45720.
58. Schreiber, S., S. Gross, A. Brandis, A. Harmelin, V. Rosenbach-Belkin, A. Scherz and Y. Salomon (2002) Local photodynamic therapy (PDT) of rat C6 glioma xenografts with Pd-bacteriopheophorbide leads to decreased metastases and increase of animal cure compared with surgery. *Int. J. Cancer* **99**, 279–285.
59. # 9421 (1996) Taurine. In *The Merck Index: An Encyclopedia of Chemicals, Drugs, and Biologicals*, 12th edition (Edited by S. Budavari, M. J. O'Neil, A. Smith, P. E. Heckelman and J. F. Kinneary), p. 1554. Merck, Whitehouse Station, NJ.
60. Redmond, H. P., P. P. Stapleton, P. Neary and D. Bouchier-Hayes (1998) Immunonutrition: the role of taurine. *Nutrition* **14**, 599–604.
61. Saransaari, P. and S. S. Oja (2000) Taurine and neural cell damage. *Amino Acids* **19**, 509–526.
62. Schaffer, S. W., J. B. Lombardini and J. Azuma (2000) Interactions between the actions of taurine and angiotensin II. *Amino Acids* **18**, 305–318.
63. Hu, P., J. Yan, J. Sharifi, T. Bai, L. A. Khawli and A. L. Epstein (2003) Comparison of three different targeted tissue factor fusion proteins for inducing tumor vessel thrombosis. *Cancer Res.* **63**, 5046–5053.
64. Thorpe, P. E. (2004) Vascular targeting agents as cancer therapeutics. *Clin. Cancer Res.* **10**, 415–427.
65. Nilsson, F., H. Kosmehl, L. Zardi and D. Neri (2001) Targeted delivery of tissue factor to the ED-B domain of fibronectin, a marker of angiogenesis, mediates the infarction of solid tumors in mice. *Cancer Res.* **61**, 711–716.
66. Jain, R. K. (2003) Molecular regulation of vessel maturation. *Nat. Med.* **9**, 685–693.
67. Huang, Z., Q. Chen, N. Trncic, S. M. LaRue, P. H. Brun, B. C. Wilson, H. Shapiro and F. W. Hetzel (2004) Effects of Pd-bacteriopheophorbide (TOOKAD)-mediated photodynamic therapy on canine prostate pretreated with ionizing radiation. *Radiat. Res.* **161**, 723–731.